中國機械工程學刊第四十二卷第六期第 613~618 頁(民國一百一十年)
Journal of the Chinese Society of Mechanical Engineers, Vol.42, No.6, pp. 613~618 (2021)

A Study of Tibial Motion Accuracy using Circular and Noncircular Gears in a Transfemoral Prosthetic Knee Part 1: Tibial Motion Acquisition

Wen-Tzong Lee*, Kevin Russell**, Raj S. Sodhi**

Keywords: Prosthetic Knee, RRSS Linkage, Motion Generation, Axode Generation, Circle Fitting, Gears Design

ABSTRACT

This is the first part of a two-part work where the authors' design method for gear-based transfemoral prosthetic knees is demonstrated using knee motion data from 7 clinical knee motion studies. The purpose of this two-part work is to determine if circular gears can consistently exhibit accurate tibial motion during gait versus noncircular gears in a transfemoral prosthetic knee. In part 1, tibial positions reflecting tibial motion during gait are calculated using the knee motion data presented in the 7 clinical knee motion studies. These studies reflect factors such as participant age, gender, nationality, body mass index, gait speed and knee condition. Unlike noncircular gears, which are custom-made, circular gears can offer advantages in manufacturing cost and design simplicity since it is a standard component. However, to justify the use of circular gears in the knee design, it must be determined if it can consistently exhibit tibial motion that is as accurate as noncircular gears.

INTRODUCTION

Natural Motion of the Human Knee

The human knee joint connects the tibia and femur. These two bones are the largest in the leg. The knee can be described as a spatial joint having 6 degrees of freedom. This mobility includes 3 principal rotations about and translations along a given spatial Cartesian frame within the knee (Grood and Suntay 1983). In Figure 1, the terms δ_x, δ_y and δ_z represent the principal rotations (about the X, Y and Z-axes respectively) and Δ_x, Δ_y, and Δ_z represent the principal translations (along the X, Y and Z-axes respectively). While specific clinical terms are often used to describe knee motion, the descriptions in Fig. 1 will be used throughout this work for brevity and simplicity.

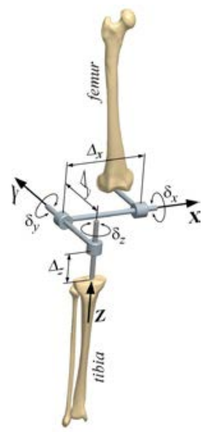

Fig. 1. Human knee displacements and rotations

Transfemoral Prosthetic Knee Design Method

A *transfemoral prosthetic knee* is the type of artificial knee used by above-the-knee amputees. The authors presented a design method for gear-based transfemoral prosthetic knees (Lee et al. 2020; Lee et al. 2018). This method includes the 4 stages as illustrated in Figure 2. This work focuses on the first stage while the part 2 work focuses on stages 2 through 4 In the first stage, positions of the tibia over knee motion are produced. These positions are represented by the spatial Cartesian coordinates of 3 points attached to the tibia. The clinical approach to acquire this data is to attach bone-mounted or skin-mounted markers to the leg and measure the point coordinates over knee motion. In this work

Paper Received June, 2020. Revised September, 2021. Accepted September, 2021. Author for Correspondence:Wen-Tzong Lee.

* *Department of Biomechatronics Engineering, National Pintung University of Science and Technology, Pingtung, 91201, Taiwan.*

** *Department of Mechanical and Industrial Engineering, New Jersey Institute of Technology, Newark, New Jersey 07102, USA*

however, tibial spatial Cartesian points over knee motion are calculated using plots for δ_x, δ_y, δ_z, Δ_x, Δ_y, and Δ_z which were obtained from 7 clinical knee motion studies. The latter procedure is presented in detail in Section 3.1.

While this work focuses exclusively on the first stage in the authors' design method (Fig. 2), the transfemoral prosthetic knee design is produced at the conclusion of the design process. Figure 3 illustrates a concept transfemoral prosthetic knee design produced from the authors' design process (Lee et al. 2020; Lee et al. 2018). The internal-external gear pair (used to exhibit natural tibial motion during gait) is included in this figure.

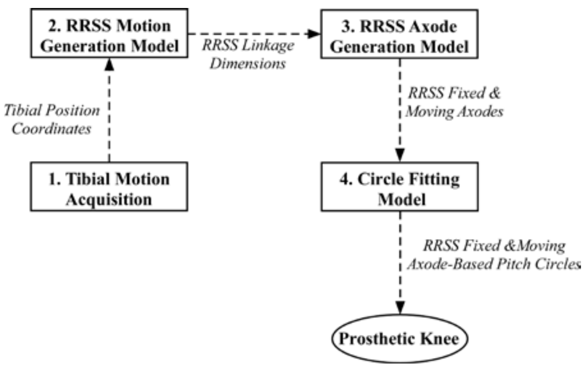

Fig. 2. Gear-based transfemoral prosthetic knee design process

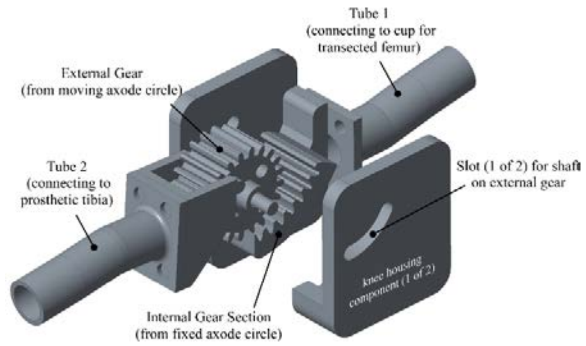

Fig. 3. Concept design produced from knee design process

Objective

This work is the first part of a two-part work where the authors' design method for gear-based transfemoral prosthetic knees is used to determine if circular gears are comparable to noncircular gears (in terms of tibial position accuracy) in a transfemoral prosthetic knee. This work demonstrates the first stage (the tibial motion acquisition stage) in the authors' design method.

EMPIRICAL HUMAN KNEE MOTION DATA

Figure 4 includes plots of average principal knee rotations and translations from the work of Benoit et. al. (2007). Six healthy subjects (all male) with an average age of 26 years and no history of knee injury or lower-limb surgery were recruited for this study. The subjects performed a series of normal walking trials along a 12-meter walkway at a self-selected pace. Five points were selected from these knee rotation and translation plots and used (in the first stage) in the authors' design method to produce the transfemoral prosthetic knee illustrated in Fig. 3 (Lee et al. 2020; Lee et al. 2018). Because 5 groups of valus for δ_x, δ_y, δ_z, Δ_x, Δ_y, and Δ_z were selected, the resulting transfemoral prosthetic knee approximates 5 tibial positions over the walking gait cycle.

Circular gears were demonstrated to be more accurate than noncircular gears using the knee motion data from Benoit et. al. (2007). This knee motion data however (representing only 6 young, healthy all-male subjects) do not reflect distinctions in human physical characteristics. Incorporating distinctions such as those due to gender, age, nationality, body mass, gait speed and knee condition would enable one to better evaluate the performance of circular versus noncircular gears in the knee design.. To account for such distinctions, knee motion data like Fig. 4 were selected from published sources that consider them.

Table 1 includes knee motion data from the work of Kozánek et. al. (2009). Eight subjects (6 males and 2 females) aged 32 to 49 years, with an average body mass index of 23.5 kg/m^2 were recruited for this study. The subjects had no history of knee injury, surgery or systemic disease. The subjects performed treadmill gait for 1 minute at a speed of 0.67 m/s.

Table 2 includes knee motion data from the work of Zhang et. al. (2015). Twenty-eight Chinese subjects (14 males and 14 females) aged 20 to 30 years with an average body mass index of 20.8 kg/m^2 were recruited for this study. All of the subjects had no history of major trauma, surgery, knee-related symptoms, or obvious disorders in their lower extremities. The subjects performed treadmill gait for 15 seconds at a speed of 0.83 m/s.

Tables 3 and 4 include knee motion data from the work of Zeng et. al. (2017). For Table 3, 26 subjects (12 males and 14 females) with early medial *knee osteoarthritis* (KOA), an average age of 53.6 years and an average body mass index of 24.0 kg/m^2 were recruited for this study. For Table 4, 38 subjects (10 males and 28 females) with severe medial knee osteoarthritis, an average age of 63.5 years and an average body mass index of 23.1 kg/m^2 were recruited for this study. The subjects all performed treadmill gait for 15 seconds at a speed of 0.56 m/s.

Tables 5 and 6 include knee motion data from the work of Zheng et. al. (2017). Nine subjects (3 males and 6 females) aged 18 to 53 years with an average body mass index of 25.0 kg/m^2 and each having a *knee meniscectomy* (KM), were recruited for this study. Four of the 9 subjects had each undergone a medial knee meniscectomy for Table 5 and 5 of the 9 the subjects had each undergone a lateral knee meniscectomy for Table 6. The subjects all performed 15°-decline, dual belt treadmill gait (recorded over a 1-second duration) at a speed of 1 m/s.

Table 7 includes knee motion data from the work of Li et. al. (2017, 2019). Ten obese subjects (2 males and 8 females) with an average age of 42.8 years and an average body mass index of 39.6 kg/m^2 were recruited for this study. The subjects all reported experienceing knee pain but also reported being able to walk without assistance. The subjects performed treadmill gait (over durations limited by knee pain) at a speed of 0.67 m/s.

So as conveyed, Tables 1 through 7 were selected from knee motion studies whose participants reflect a much broader range of physical distinctions than those reflected in the work of Benoit et. al.. This data will be utilized in the first stage of the authors' design method to calculate tibial positions as spatial Cartesian coordinates.

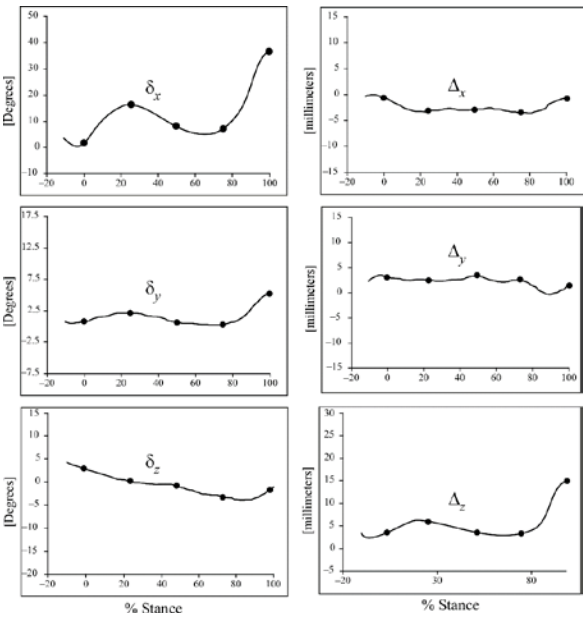

Fig. 4. Average knee rotation and translation plots and selected values

Table 1. Selected knee rotations and translation during treadmill gait (Kozánek et. al.)

Pos.	δ_x [deg]	δ_y [deg]	δ_z [deg]	Δ_x [mm]	Δ_y [mm]	Δ_z [mm]
1	1.00	3.53	−1.50	3.21	−2.67	34.30
2	9.00	4.47	4.80	5.13	−0.17	33.40
3	22.00	5.07	3.00	1.34	−0.17	33.70
4	30.00	5.46	5.10	1.93	1.17	34.45
5	37.00	5.93	7.50	2.57	2.50	35.32

Table 2. Selected knee rotations and translation during treadmill gait (Zhang et. al.)

Pos.	δ_x [deg]	δ_y [deg]	δ_z [deg]	Δ_x [mm]	Δ_y [mm]	Δ_z [mm]
1	5.20	−0.73	−0.26	8.00	−2.25	−0.10
2	7.20	0.55	1.18	6.63	0.25	4.10
3	24.40	0.78	−1.07	5.50	4.75	11.00
4	47.60	1.75	1.00	7.00	2.00	12.20
5	55.36	1.08	2.08	10.25	−0.25	11.90

Table 3. Selected knee rotations and translation during treadmill gait with moderate KOA (Zeng et. al.)

Pos.	δ_x [deg]	δ_y [deg]	δ_z [deg]	Δ_x [mm]	Δ_y [mm]	Δ_z [mm]
1	7.67	−0.78	−0.82	0.17	2.98	−3.00
2	11.90	0.17	0.40	0.60	5.70	2.00
3	26.75	1.88	1.40	1.16	9.69	−0.10
4	38.00	3.21	2.30	2.44	11.06	−0.90
5	43.67	2.64	2.30	3.64	11.06	−0.70

Table 4. Selected knee rotations and translation during treadmill gait with severe KOA (Zeng et. al.)

Pos.	δ_x [deg]	δ_y [deg]	δ_z [deg]	Δ_x [mm]	Δ_y [mm]	Δ_z [mm]
1	11.90	−3.25	−3.50	−2.84	5.15	−0.80
2	11.90	−2.59	−2.10	−1.64	5.70	0.50
3	21.35	−1.64	−0.80	−1.62	8.04	0.30
4	29.90	−0.49	0.80	−1.40	9.33	−0.30
5	34.49	−0.31	0.80	−1.24	9.41	−0.50

Table 5. Selected knee rotations and translation during treadmill gait with medial KM (Zheng et. al.)

Pos.	δ_x [deg]	δ_y [deg]	δ_z [deg]	Δ_x [mm]	Δ_y [mm]	Δ_z [mm]
1	−4.00	−1.78	−1.43	0.23	−7.15	−29.10
2	1.25	−2.56	−0.90	0.67	−3.85	−29.25
3	12.00	−4.84	3.30	1.13	−0.85	−28.88
4	32.00	−5.01	3.83	−0.23	1.85	−28.88
5	36.75	−5.28	6.63	−0.23	2.00	−28.95

Table 6. Selected knee rotations and translation during treadmill gait with lateral KM (Zheng et. al.)

Pos.	δ_x [deg]	δ_y [deg]	δ_z [deg]	Δ_x [mm]	Δ_y [mm]	Δ_z [mm]
1	18.13	1.81	−1.69	4.50	14.68	−21.75
2	31.00	2.08	−2.83	2.25	16.70	−19.50
3	38.13	2.43	−2.65	0.75	18.95	−18.30
4	46.50	2.60	−6.33	−0.15	18.05	−17.40
5	48.63	1.99	−6.33	−0.38	17.15	−17.25

Table 7. Selected knee rotations and translation during treadmill gait (Li et. al.)

Pos.	δ_x [deg]	δ_y [deg]	δ_z [deg]	Δ_x [mm]	Δ_y [mm]	Δ_z [mm]
1	11.50	−3.52	2.15	−3.68	1.50	29.80
2	13.10	−3.60	0.88	−3.40	2.50	29.50
3	14.00	−3.12	0.75	−3.24	2.00	29.40
4	19.00	−3.04	1.25	−3.00	2.40	29.60
5	27.50	−3.20	1.50	−2.60	3.00	30.10

TIBIOFEMORAL POSITION CALCULATION

The motion generation model used in the second stage (Fig. 2) requires point coordinates in spatial Cartesian form. The knee motion data in Tables 1 through 7 was used to calculate the coordinates of three points (defined as points **p**, **q** and **r**). This data defines the position of the tibia bone with respect to the femur bone during gait.

Equation (1) is a 6-DOF displacement matrix expressed in terms of δ_x, δ_y, δ_z, Δ_x, Δ_y, and Δ_z. This matrix is the product of the rotation matrices about the X, Y and Z-axes combined with a column vector that includes the translations along the X, Y and Z-axes. Equations (2) through (4) are used to calculate the spatial Cartesian coordinates for the 3 points that define the position of the tibia during gait. The values of **p**, **q** and **r** in Equ. (2) through (4) can be arbitrary since the data in Tables 1 through 7 are *displacement* values. In this work, they are assigned values of $\mathbf{p} = \begin{bmatrix} -11 & 60 & 181 & 1 \end{bmatrix}^T$, $\mathbf{q} = \begin{bmatrix} 33 & 58 & 182 & 1 \end{bmatrix}^T$ and $\mathbf{r} = \begin{bmatrix} 34 & 55 & 128 & 1 \end{bmatrix}^T$ millimeters. Because the spatial position of a body can be defined using the natural spatial coordinates of three arbitrary points, the values assigned to **p**, **q** and **r** can be arbitrarily assigned. The only restriction to specifying values for these points is that is that they should not lie on a common line.

$$\begin{bmatrix} M_j \end{bmatrix} = \begin{bmatrix} \cos\delta_{yj}\cos\delta_{zj} & -\cos\delta_{yj}\sin\delta_{zj} & \sin\delta_{yj} & \Delta_{xj} \\ \sin\delta_{xj}\sin\delta_{yj}\cos\delta_{zj}+\cos\delta_{xj}\sin\delta_{zj} & \cos\delta_{xj}\cos\delta_{zj}-\sin\delta_{xj}\sin\delta_{yj}\sin\delta_{zj} & -\sin\delta_{xj}\cos\delta_{yj} & \Delta_{yj} \\ \sin\delta_{xj}\sin\delta_{zj}-\cos\delta_{xj}\sin\delta_{yj}\cos\delta_{zj} & \cos\delta_{xj}\sin\delta_{yj}\sin\delta_{zj}+\sin\delta_{xj}\cos\delta_{zj} & \cos\delta_{xj}\cos\delta_{yj} & \Delta_{zj} \\ 0 & 0 & 0 & 1 \end{bmatrix}, \tag{1}$$

$$\mathbf{p}_j = \begin{bmatrix} M_j \end{bmatrix}\mathbf{p} \quad j = 1,2,\ldots 5, \tag{2}$$

$$\mathbf{q}_j = \begin{bmatrix} M_j \end{bmatrix}\mathbf{q} \quad j = 1,2,\ldots 5, \tag{3}$$

$$\mathbf{r}_j = \begin{bmatrix} M_j \end{bmatrix}\mathbf{r} \quad j = 1,2,\ldots 5. \tag{4}$$

TIBIA POSITIONS DURING GAIT

The point coordinates for 5 tibial positions are given in Tables 8 through 14. This position data was calculated using the knee motion data in Tables 1 through 7 respectively and Equations (2) through (4). Tables 8 through 14 represent both the output from the first stage and the input for the second stage in the authors' knee design method (Fig. 2).

Table 8. Calculated tibial position coordinates using knee motion data from Kozánek et. al.

Pos.	**p** [mm]	**q** [mm]	**r** [mm]
1	4.94, 54.43, 216.56	48.86, 51.30, 214.80	46.45, 49.22, 160.80
2	3.30, 29.55, 222.07	47.26, 31.60, 219.93	44.30, 37.17, 166.20
3	3.27, −13.15, 224.25	47.23, −11.78, 221.68	43.61, 5.67, 170.61
4	2.93, −38.79, 221.22	46.83, −35.53, 219.42	42.95, −1.10, 171.31
5	2.63, −60.65, 215.58	46.39, −55.52, 215.02	42.18, −25.38, 170.30

Table 9. Calculated tibial position coordinates using knee motion data from Zhang et. al.

Pos.	**p** [mm]	**q** [mm]	**r** [mm]
1	−5.02, 41.16, 185.45	38.96, 38.83, 186.80	40.63, 40.73, 132.77
2	−3.87, 36.84, 191.27	40.17, 35.68, 191.71	40.71, 39.50, 137.75
3	−1.93, −15.25, 200.81	44.04, −17.99, 200.01	42.25, 1.57, 149.58
4	0.49, −91.55, 178.60	44.53, −92.12, 177.46	43.93, −54.25, 138.84
5	0.48, −115.49, 163.91	44.53, −115.86, 163.68	44.63, −73.10, 130.54

Table 10. Calculated tibial position coordinates using knee motion data from Zeng et. al. (moderate KOA)

Pos.	**p** [mm]	**q** [mm]	**r** [mm]
1	−12.44, 38.45, 184.26	31.51, 35.63, 185.49	33.21, 39.85, 131.59
2	−10.28, 27.00, 191.50	33.73, 25.17, 192.00	34.59, 33.38, 138.54
3	−5.36, −18.60, 188.68	38.69, −19.22, 187.87	37.99, 2.43, 138.31
4	−0.80, −53.76, 178.74	43.23, −53.04, 177.44	41.32, −22.14, 133.08
5	−1.41, −71.17, 171.62	42.64, −70.62, 170.72	41.27, −35.48, 129.62

Table 11. Calculated tibial position coordinates using knee motion data from Zeng et. al. (severe KOA)

Pos.	**p** [mm]	**q** [mm]	**r** [mm]
1	−20.41, 27.23, 188.11	23.26, 21.93, 190.55	27.14, 30.05, 137.21
2	−18.59, 27.56, 189.49	25.22, 23.41, 191.66	28.54, 31.56, 138.29
3	−16.95, −1.71, 190.44	26.98, −4.96, 191.59	29.47, 11.87, 140.24
4	−14.80, −28.97, 186.34	29.21, −30.86, 186.85	30.72, −6.53, 138.56
5	−14.04, −43.72, 182.52	29.98, −45.56, 182.75	31.31, −17.45, 136.56

Table 12. Calculated tibial position coordinates using knee motion data from Zheng et. al. (medial KM)

Pos.	p [mm]	q [mm]	r [mm]
1	−14.88, 65.56, 146.88	29.00, 62.64, 149.45	31.60, 55.86, 95.84
2	−17.46, 52.37, 152.39	26.41, 49.61, 155.29	29.78, 47.77, 101.34
3	−28.52, 19.88, 158.67	15.28, 19.42, 163.39	21.00, 27.72, 110.24
4	−30.96, −42.86, 154.26	12.82, −44.63, 158.87	18.73, −18.66, 111.78
5	−34.64, −58.12, 149.05	9.02, −58.66, 154.93	15.32, −28.85, 110.23

Table 13. Calculated tibial position coordinates using knee motion data from Zheng et. al. (lateral KM)

Pos.	**p** [mm]	**q** [mm]	**r** [mm]
1	1.00, 15.61, 169.22	44.93, 12.60, 167.82	44.14, 26.52, 115.56
2	0.78, −24.78, 166.94	44.63, −28.05, 164.29	43.53, −2.85, 116.44
3	0.20, −45.36, 161.55	44.07, −48.00, 158.39	42.64, −17.07, 114.04
4	3.74, −71.37, 151.34	47.25, −75.36, 145.71	45.47, −38.34, 106.31
5	1.58, −78.48, 148.07	45.10, −82.62, 142.61	43.89, −44.15, 104.60

Table 14. Calculated tibial position coordinates using knee motion data from Li et. al.

Pos.	**p** [mm]	**q** [mm]	**r** [mm]
1	−28.01, 23.99, 217.91	15.89, 22.92, 221.47	20.31, 30.75, 168.13
2	−26.66, 19.99, 218.27	17.22, 17.85, 221.64	21.65, 27.14, 168.53
3	−24.86, 16.51, 218.62	19.04, 14.30, 221.57	23.02, 24.44, 168.58
4	−24.89, 0.26, 219.33	19.03, −1.81, 222.15	22.96, 12.91, 170.24
5	−25.25, −27.18, 217.34	18.66, −29.52, 220.01	22.75, −7.29, 170.87

DISCUSSION

While groups of 5 tibia positions are considered in Tables 8 through 14, the authors' design method can theoretically accommodate an indefinite number of positions. The limiting actor for the maximum number of tibia positions the user can specify is the computing capacity needed to solve the RRSS motion generation model in the second stage of the author's design method.

CONCLUSION

Using the knee motion data from 7 clinical knee motion studies, 7 groups of tibial positions during gait were successfully calculated. Unlike the clinical knee motion study from Benoit et. al. (2007), the knee motion studies used in this work consider factors such as participant age, gender, nationality, body mass, gait speed and knee condition. This work is the first part of a two-part work where the authors' design method for gear-based transfemoral prosthetic knees is used to determine if circular gears are comparable to noncircular gears (in terms of tibial position accuracy) in a transfemoral prosthetic knee. This work demonstrates the first stage (the tibial motion acquisition stage) in the authors' design method. In the second part of this two-part work, the remaining stages (the RRSS motion generation, RRSS axode generation and curve fitting stages) are demonstrated.

REFERENCES

Benoit, D. L., Ramsey, D. K., Lamontagne, M., Xu, L., Wretenberg, P., and Renström P.,. "In Vivo Knee Kinematics during Gait Reveals New Rotation Profiles and Smaller Translations,"; Clinical Orthopaedics and Related Research, Vol. 454, No.1, pp. 81-88(2007).

Grood, E. S. and Suntay, W. J., "A Joint Coordinate System for the Clinical Description of Three-dimensional Motions: Application to the Knee. Journal of Biomechanical Engineering,"; Vol. 105 No.2, pp. 136-144(1983).

Kozánek, M., Hosseini, A., Liu, F., Van, de Velde S. K., Gill, T. J., Rubash, H. E. and Li, G., "Tibiofemoral Kinematics and Condylar Motion during the Stance Phase of Gait,"; Journal of Biomechanics, Vol.42, No.12, pp. 1877-1884(2009).

Lee, W., "An Evaluation of Spatial and Spherical Motion Generation for Application in Knee Motion Analysis and Simulation,"; Journal of the Chinese Society of Mechanical Engineers, Vol. 41, No. 2, pp. 221-228(2020).

Lee, W., Russell, K. and Sodhi, R. S., "On Transfemoral Prosthetic Knee Design for Natural Human Knee Motion,"; Recent Patents on Mechanical Engineering, Vol.13, No.1, pp. 49-59(2020).

Lee, W., Russell, K., D'Alessio, J. and Sodhi, R. S., "Method of Designing and Manufacturing Artificial Joint,"; TW Patent I642419(2018).

Li, J., Tsai, T., Felson, D. T., Li, G. and Lewis, C. L., "Six Degree-of-Freedom Knee Joint Kinematics in Obese Individuals with Knee Pain during

Gait,"; PLoS ONE. Vol.12, No.3, pp. e0174663(2017).

Li, J., Tsai, T., Felson, D. T., Li, G. and Lewis, C. L., "Correction: Six Degree-of-Freedom Knee Joint Kinematics in Obese Individuals with Knee Pain during Gait,"; PLoS ONE. Vol.14, No.2, pp. e0213084(2019).

Zeng, X., Ma, L., Lin, Z., Huang, W., Huang, Z., Zhang, Y. and Mao, C., "Relationship Between Kellgren-Lawrence Score and 3D Kinematic Gait Analysis of Patients with Medial Knee Osteoarthritis Using a New Gait System,"; Scientific Reports. Vol.7, No.1, pp. 4080(2017).

Zhang, Y., Yao, Z., Wang, S., Huang, W., Ma, L, Huang, H., and Xia, H., "Motion Analysis of Chinese Normal Knees during Gait Based on a Novel Portable System,"; Gait Posture, Vol.41, No.3, pp. 763-768(2015).

Zheng, L., Carey, R., Thorhauer, E., Tashman, S., Harner, C. and Zhang, X., "In Vivo Tibiofemoral Skeletal Kinematics and Cartilage Contact Arthrokinematics During Decline Walking After Isolated Meniscectomy,"; Medical Engineering and Physics, Vol.51, pp. 41-48(2018).

經股人工膝關節使用圓形與非圓形齒輪進行脛骨運動精度的研究
第一部分：脛骨運動擷取

李文宗
國立屏東科技大學 生物機電工程學系

羅素凱文　索德　里拉茲
紐澤西理工學院 機械與工業工程學系

摘要

這是兩個相關研究的第一部分。作者們使用七項臨床膝關節運動研究的膝關節運動數據，示範應用齒輪為基礎的經股人工膝關節的設計方法。這兩個相關研究的主要目的是測試圓形齒輪與非圓形齒輪在經股人工膝關節的步態過程中，是否都能夠始終如一地表現出準確的脛骨運動。在第一部分中，使用七項臨床膝關節運動研究提供的膝關節運動數據，計算反映步態過程中脛骨運動的位置。這些研究反映了參與者的年齡、性別、國籍、體重指數、步態速度與膝關節狀況等因素。與需要客制化的非圓形齒輪不同的地方，圓形齒輪在製造成本和設計簡易性方面均具有優勢，因為它是屬於標準製造的零件。然而，為了證明在膝關節設計中使用圓形齒輪是合適的，必須確定它是否可以始終如一地表現出與非圓形齒輪一樣準確的脛骨運動。

中國機械工程學刊第四十二卷第六期第 619~630 頁(民國一百一十年)
Journal of the Chinese Society of Mechanical Engineers, Vol.42, No.6, pp. 619~630 (2021)

A Study of Tibial Motion Accuracy using Circular and Noncircular Gears in a Transfemoral Prosthetic Knee Part 2: Motion and Axode Generation and Curve Fitting

Wen-Tzong Lee*, Kevin Russell**, Raj S. Sodhi**

Keywords: Prosthetic Knee, RRSS Linkage, Motion Generation, Axode Generation, Circle Fitting, Gears Design

ABSTRACT

This is the second part of a two-part work where the authors' design method for gear-based transfemoral prosthetic knees is demonstrated using knee motion data from 7 clinical knee motion studies. The purpose of this two-part work is to determine if circular gears can consistently exhibit accurate tibial motion during gait versus noncircular gears in a transfemoral prosthetic knee. In part 2, RRSS linkages are calculated to approximate the tibial positions produced in part 1. The axodes for these linkages are also generated and circle dimensions are calculated that best fit the centrodes. These circles become the pitch circles for gear pairs to be included in the prosthetic knee design. Lastly, a tibial position accuracy comparison between the knee design using circular gears versus noncircular gears is made. Unlike noncircular gears, which are custom-made, circular gears can offer advantages in manufacturing cost and design simplicity since it is a standard component. However, to justify the use of circular gears in the knee design, it must be determined if it can consistently exhibit tibial motion that is as accurate as noncircular gears.

INTRODUCTION

Paper Received June, 2020. Revised September, 2021. Accepted September, 2021. Author for Correspondence:Wen-Tzong Lee.

* *Department of Biomechatronics Engineering, National Pintung University of Science and Technology, Pingtung, 91201, Taiwan.*

** *Department of Mechanical and Industrial Engineering, New Jersey Institute of Technology, Newark, New Jersey 07102, USA*

Transfemoral Prosthetic Knee Design Method

The authors presented a design method for gear-based transfemoral prosthetic knees (Lee et al. 2020; Lee et al. 2018). This method includes the 4 stages as illustrated in Figure 1. In part 1 of this two-part work, the first stage (tibial motion acquisition) was completed. In this work, the remaining stages are completed.

In the second stage the tibial spatial Cartesian points are incorporated (as precision positions) in a motion generation model for the spatial four-bar *Revolute-Revolute-Spherical-Spherical* or RRSS linkage. The dimensions for an RRSS linkage with a coupler link that approximates the tibial spatial Cartesian points are calculated in this stage. Figure 2 includes the prescribed and calculated RRSS linkage dimensions and displacement angles.

In the third stage, the dimensions of the synthesized RRSS linkage are incorporated in an axode generation model. The results of this stage are the fixed and moving axodes for the RRSS linkage. The coupler motion achieved by the synthesized RRSS linkage is replicated by the rolling motion of the moving axode over the fixed axode. Because the RRSS coupler motion is replicated, the tibial spatial Cartesian points achieved by the mechanism are also reproduced. The fixed and moving axodes can be used as pitch curves for a gear pair. Using a gear pair, the rolling motion of the moving axode over the fixed axode become the rolling motion of the moving axode gear over the fixed axode gear.

Because the RRSS linkage axodes are not perfect circles, they would become pitch curves for *noncircular* gears if used as calculated in the third stage. In the fourth stage, the centers and radii of circles that best fit the fixed and moving axodes are calculated. These are the pitch circles for true circular gears for the prosthetic knee design. Figure 3 illustrates a prosthetic knee design produced from the authors' design method (Lee et al. 2020; Lee et al.

2018). The rolling motion of the external gear over the internal gear approximates the prescribed tibial positions.

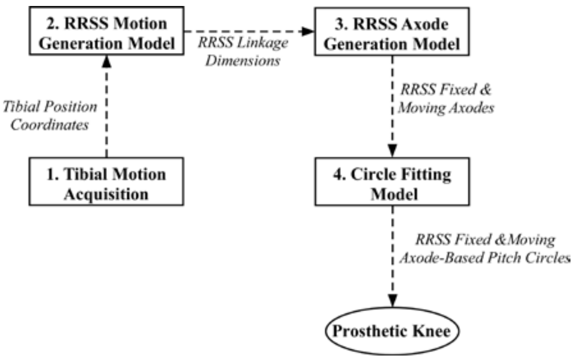

Fig. 1. Gear-based transfemoral prosthetic knee design process

Objective

This work is the second part of a two-part work where the authors' design method for gear-based transfemoral prosthetic knees is used to determine if circular gears are comparable to noncircular gears (in terms of tibial position accuracy) in a transfemoral prosthetic knee. This work demonstrates the stages 2 through 4 (the RRSS motion generation, axode generation and circle fitting stages) in the authors' design method.

RRSS LINKAGE MOTION GENERATION

The RRSS linkage is illustrated in Fig. 2. It is a four-link spatial mechanism having 2 degrees of freedom. One degree of freedom however is the rotation of the follower link about its own length. This degree of freedom is known as a *passive degree of freedom* because it does not compromise the overall kinematics of the RRSS linkage (giving it an effective mobility of 1).

The authors presented a constrained optimization model for the motion generation of defect-free RRSS linkages (Russell and Shen 2013). While the reader can find a full description of this optimization model in the referenced work, the model's objective function is

$$f(\mathbf{X}) = \frac{1}{2}\sum_{j=2}^{5}\left\{\left\|\mathbf{p}_j^* - \mathbf{p}_j\right\|^2 + \left\|\mathbf{q}_j^* - \mathbf{q}_j\right\|^2 + \left\|\mathbf{r}_j^* - \mathbf{r}_j\right\|^2\right\}, \quad (1)$$

where the calculated RRSS linkage dimensions are $\mathbf{X} = \left(\mathbf{a}_0, \mathbf{u}_{\mathbf{a}_0}, \mathbf{a}_1, \mathbf{u}_{\mathbf{a}_1}, \mathbf{b}_0, \mathbf{b}_1, \theta_j, \alpha_j\right)$. As illustrated in Fig. 2, $\mathbf{a}_0$ and $\mathbf{b}_0$ are the mechanism fixed pivots while $\mathbf{a}_1$ and $\mathbf{b}_1$ are the mechanism moving pivots. Unit vectors $\mathbf{u}_{\mathbf{a}_0}$ and $\mathbf{u}_{\mathbf{a}_1}$ are the revolute joint axis orientations at $\mathbf{a}_1$ and $\mathbf{b}_1$ respectively while θ_j and α_j are the angular displacement of the crank and coupler links respectively (Fig. 2). In Equation (1), the prescribed tibia positions ($\mathbf{p}_j$, $\mathbf{q}_j$ and $\mathbf{r}_j$) are calculated from Equations (2) through (4) (in the part 1 work) while $\mathbf{p}_j^*$, $\mathbf{q}_j^*$ and $\mathbf{r}_j^*$ are tibia positions achieved by the synthesized RRSS linkage. In Equ. (1), the difference between the two groups of tibia positions is minimized.

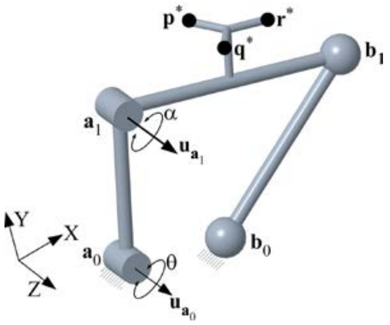

Fig. 2. RRSS linkage dimensions

RRSS LINKAGE AXODE GENERATION

An RRSS linkage with sections of its fixed and moving axodes are illustrated in Fig. 3. Axodes for the RRSS linkage are analogous to what *centrodes* are for the planar four-bar linkage. Therefore, like centrodes, the coupler motion of the RRSS linkage is replicated by rolling its moving axode over its fixed axode.

The authors presented a method to calculate the fixed and moving axodes for the RRSS linkage (Shen et al. 2011). While the reader can find a detailed description of this calculation method in the referenced work, the equation to calculate a single point ($\mathbf{x}$) on each instant screw axis is

$$\mathbf{x} = \mathbf{b}_0 + \frac{\left[\left(\mathbf{a}-\mathbf{a}_0\right)\times\mathbf{u}_{\mathbf{a}_0}\right]\cdot\left(\mathbf{b}_0-\mathbf{a}_0\right)}{\left[\left(\mathbf{a}-\mathbf{a}_0\right)\times\mathbf{u}_{\mathbf{a}_0}\right]\cdot\left(\mathbf{b}_0-\mathbf{b}\right)}\left(\mathbf{b}-\mathbf{b}_0\right), \quad (2)$$

where $\mathbf{x} = \left(x, y, z\right)$.

To produce axodes that suitable for gear design, the unit vectors for each instant screw axis in the centrode and the RRSS joint axes $\mathbf{u}_{\mathbf{a}_0}$ and $\mathbf{u}_{\mathbf{a}_1}$ must be parallel. To ensure this, the optimization model for RRSS motion generation includes the constraint $\left(\mathbf{u}_{\mathbf{a}_0}\right)^T\left(\mathbf{u}_{\mathbf{a}_1}\right) - 1 = 0$. This constraint makes $\mathbf{u}_{\mathbf{a}_0}$ and $\mathbf{u}_{\mathbf{a}_1}$ parallel. Making $\mathbf{u}_{\mathbf{a}_0}$ and $\mathbf{u}_{\mathbf{a}_1}$ parallel also ensures that each instant screw axis point calculated from Equ. (2) lies on the X'-Y' plane illustrated in Fig. 3 (making $\mathbf{x} = \left(x, y, 0\right)$ in Equ. (2)). The X'-Y' plane is a local plane that includes $\mathbf{a}_0$, $\mathbf{a}_1$ and is orthogonal to $\mathbf{u}_{\mathbf{a}_0}$ and $\mathbf{u}_{\mathbf{a}_1}$ (Fig. 3).

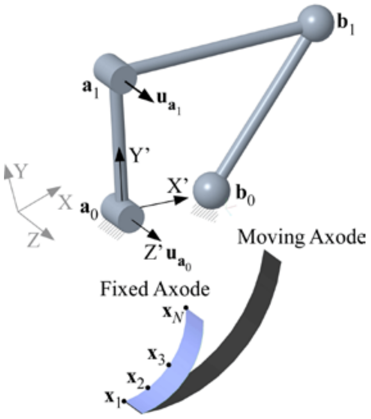

Fig. 3. RRSS linkage with its fixed and moving axode sections

GEAR PITCH CIRCLE CALCULATION

The *method of least squares* was used to calculate the radius (r) and center coordinates (h , k) of circles that result in the minimum error solution for Equation (3). These gear circles replace the noncircular RRSS axodes calculated in the third stage of the design process. The coordinates of the RRSS axode points calculated from Equ. (3) are the x_i and y_i . Therefore, minimizing Equ. (3) produces the gear pitch circles that best fit the RRSS axodes.

$$F\left(h,k,r\right)=\sum_{i=1}^{N}\left[\left(x_i-h\right)^2+\left(y_i-k\right)^2-r^2\right]^2 . \qquad (3)$$

EXAMPLES

Using Tibial Positions Calculated from Kozánek et. al.

Table 1 includes both the initial and calculated dimensions from the authors' RRSS motion generation model. The precision positions used in this example appear in Table 8 in the part 1 work. Table 1 represents both the output from the second stage and the input for the third stage in the authors' knee design method. The synthesized RRSS linkage is illustrated in Figure 4 and the tibia position coordinates achieved by this linkage are included in Table 2.

In Figure 5, the fixed and moving axode points are illustrated in the X'-Y' plane. These points were calculated using Equation (2). In Fig. 4, the spatial representations of the fixed and moving axode sections are also illustrated. The X'-Y' plane axode point coordinates represent both the output from the third stage and the input for the fourth stage in the authors' knee design method.

Figure 5 also includes the calculated pitch circle dimensions. These circle dimensions represent the output from the fourth stage in the authors' knee design method and are used in gear selection for the prosthetic knee. The tibia position coordinates (also represented by $\mathbf{p}_j^*$, $\mathbf{q}_j^*$ and $\mathbf{r}_j^*$) achieved by circular gears with calculated pitch circle dimensions are included in Table 3.

Table 1. Initial and calculated RRSS linkage dimensions

Variable	Initial Value	Calculated Value
$\mathbf{a}_0$	1, 0, 0	0.80, −0.49, 0.91
$\mathbf{a}_1$	1, 10, 0	1.33, 10.07, −0.23
$\mathbf{u}_{\mathbf{a}_0}$	1, 0, 0	0.9044, 0.0004, 0.4269
$\mathbf{u}_{\mathbf{a}_1}$	1, 0, 0	0.9044, 0.0004, 0.4269
$\mathbf{b}_0$	1, 0, 5	0.79, 0.61, 3.64
$\mathbf{b}_1$	1, 15, 7.5	1.04, 14.81, 8.21
θ_2~θ_5 [deg]	5, 10, 15, 20	9.83, 27.07, 36.08, 42.89
α_2~α_5 [deg]	−1, −2, −3, −4	−3.16, −7.60, −9.10, −9.72

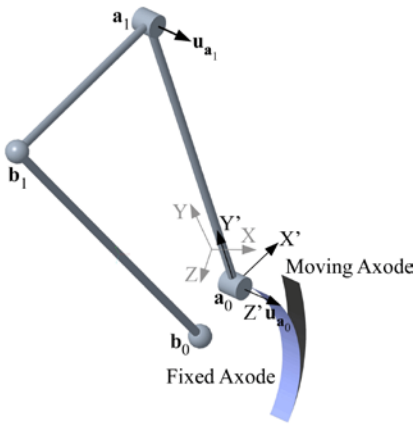

Fig. 4 Synthesized RRSS linkage with fixed and moving axode sections

Table 2. Tibial position coordinates achieved by the synthesized RRSS linkage

Pos.	$\mathbf{p}^*$ [mm]	$\mathbf{q}^*$ [mm]	$\mathbf{r}^*$ [mm]
1	4.94, 54.43, 216.56	48.86, 51.30, 214.80	46.45, 49.22, 160.80
2	2.54, 31.59, 221.68	46.55, 30.85, 219.71	44.10, 34.34, 165.79
3	1.30, −13.51, 224.35	45.16, −9.68, 222.69	41.88, 4.29, 170.53
4	2.68, −39.93, 221.46	46.25, −33.48, 220.41	42.01, −13.65, 170.26
5	4.96, −61.21, 216.64	48.19, −52.69, 216.33	42.93, −28.28, 168.34

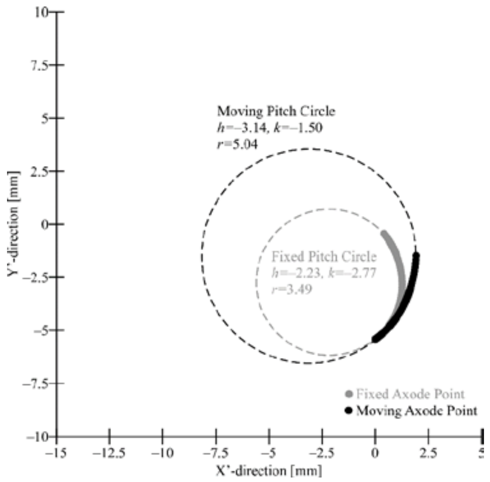

Fig. 5. RRSS linkage fixed and moving axode points (in X'-Y' plane) and gear pitch circles

Table 3. Tibial position coordinates achieved by the transfemoral prosthetic knee with circular gears

Pos.	$\mathbf{p}^*$ [mm]	$\mathbf{q}^*$ [mm]	$\mathbf{r}^*$ [mm]
1	4.94, 54.43, 216.56	48.86, 51.30, 214.80	46.45, 49.22, 160.80
2	2.67, 31.95, 221.40	46.68, 31.21, 219.44	44.23, 34.67, 165.51
3	1.50, −13.69, 223.92	45.35, −9.73, 222.29	42.03, 4.53, 170.21
4	2.79, −38.87, 221.23	46.35, −32.38, 220.19	42.09, −12.43, 170.09
5	5.09, −61.00, 216.36	48.29, −52.31, 216.11	42.94, −27.53, 168.32

Using Tibial Positions Calculated from Zhang et. al.

Table 4 includes both the initial and calculated dimensions from the authors' RRSS motion generation model. The precision positions used in this example appear in Table 9 in the part 1 work. Table 4 represents both the output from the second stage and the input for the third stage in the authors' knee design method. The synthesized RRSS linkage is illustrated in Figure 6 and the tibia position coordinates achieved by this linkage are included in Table 5.

In Figure 7, the fixed and moving axode points are illustrated in the X'-Y' plane. These points were calculated using Equation (2). In Fig. 6, the spatial representations of the fixed and moving axode sections are also illustrated. The X'-Y' plane axode point coordinates represent both the output from the third stage and the input for the fourth stage in the authors' knee design method.

Figure 7 also includes the calculated pitch circle dimensions. These circle dimensions represent the output from the fourth stage in the authors' knee design method and are used in gear selection for the prosthetic knee. The tibia position coordinates (also represented by $\mathbf{p}_j^*$, $\mathbf{q}_j^*$ and $\mathbf{r}_j^*$) achieved by circular gears with calculated pitch circle dimensions are included in Table 6.

Table 4. Initial and calculated RRSS linkage dimensions

Variable	Initial Value	Calculated Value
$\mathbf{a}_0$	1, −10, 0	0.53, −11.04, 0.47
$\mathbf{a}_1$	1, 0, 0	0.14, 0.96, 0.83
$\mathbf{u}_{\mathbf{a}_0}$	1, 0, 0	0.9964, 0.0300, 0.0791
$\mathbf{u}_{\mathbf{a}_1}$	1, 0, 0	0.9964, 0.0300, 0.0791
$\mathbf{b}_0$	1, −10, 5	1.34, −9.66, 3.56
$\mathbf{b}_1$	1, 5, 7.5	2.05, 3.38, 7.40
θ_2~θ_5 [deg]	1, 2, 3, 4	2.13, 27.07, 51.97, 58.82
α_2~α_5 [deg]	−1, −2, −3, −4	−0.97, −10.20, −12.17, −10.75

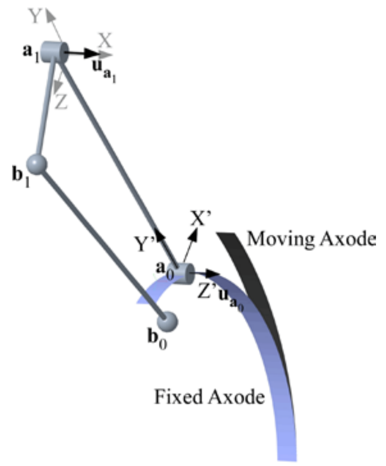

Fig. 6 Synthesized RRSS linkage with fixed and moving axode sections

Table 5. Tibial position coordinates achieved by the synthesized RRSS linkage

Pos.	$\mathbf{p}^*$ [mm]	$\mathbf{q}^*$ [mm]	$\mathbf{r}^*$ [mm]
1	−5.02, 41.16, 185.45	38.96, 38.83, 186.80	40.63, 40.73, 132.77
2	−5.00, 37.39, 186.67	38.98, 35.11, 187.95	40.61, 38.10, 133.96
3	−4.03, −15.65, 194.61	40.00, −17.21, 194.99	40.97, 0.30, 143.82
4	−0.42, −91.14, 177.82	43.63, −91.26, 177.33	43.19, −55.24, 136.98
5	1.38, -115.44, 164.39	45.42, -114.97, 163.73	44.37, -73.55, 128.95

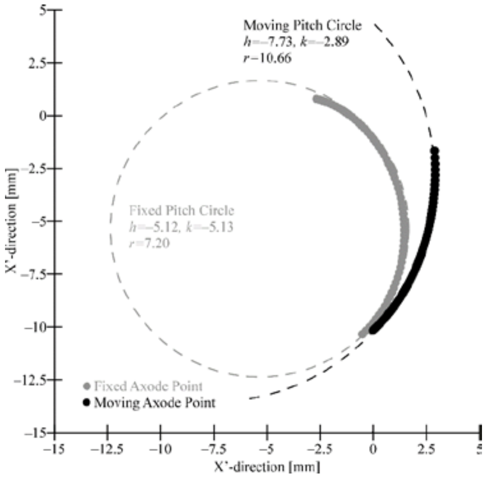

Fig. 7. RRSS linkage fixed and moving axode points (in X'-Y' plane) and gear pitch circles

Table 6. Tibial position coordinates achieved by the transfemoral prosthetic knee with circular gears

Pos.	$\mathbf{p}^*$ [mm]	$\mathbf{q}^*$ [mm]	$\mathbf{r}^*$ [mm]
1	−5.02, 41.16, 185.45	38.96, 38.83, 186.80	40.63, 40.73, 132.77
2	−4.99, 36.47, 186.88	38.99, 34.20, 188.14	40.61, 37.50, 134.17
3	−4.01, −15.90, 194.47	40.01, −17.41, 194.81	40.95, 0.73, 143.86
4	-0.48, -91.87, 178.80	43.57, -91.89, 178.27	43.02, -54.81, 138.89
5	1.31, -116.85, 165.62	45.36, -116.25, 164.94	44.17, -73.73, 131.52

Using Knee Motion Data from Zeng et. al. (moderate KOA)

Table 7 includes both the initial and calculated dimensions from the authors' RRSS motion generation model. The precision positions used in this example appear in Table 10 in the part 1 work. Table 7 represents both the output from the second stage and the input for the third stage in the authors' knee design method. The synthesized RRSS linkage is illustrated in Figure 8 and the tibia position coordinates achieved by this linkage are included in Table 8.

In Figure 9, the fixed and moving axode points are illustrated in the X'-Y' plane. These points were calculated using Equation (2). In Fig. 8, the spatial representations of the fixed and moving axode sections are also illustrated. The X'-Y' plane axode point coordinates represent both the output from the third stage and the input for the fourth stage in the authors' knee design method.

Figure 9 also includes the calculated pitch circle dimensions. These circle dimensions represent the output from the fourth stage in the authors' knee design method and are used in gear selection for the prosthetic knee. The tibia position coordinates (also represented by $\mathbf{p}_j^*$, $\mathbf{q}_j^*$ and $\mathbf{r}_j^*$) achieved by circular gears with calculated pitch circle dimensions are included in Table 9.

Table 7. Initial and calculated RRSS linkage dimensions

Variable	Initial Value	Calculated Value
$\mathbf{a}_0$	1, 0, 0	1.53, −0.47, 1.76
$\mathbf{a}_1$	1, 10, 0	0.86, 10.03, −0.85
$\mathbf{u}_{\mathbf{a}_0}$	1, 0, 0	0.9787, 0.1061, 0.1759
$\mathbf{u}_{\mathbf{a}_1}$	1, 0, 0	0.9787, 0.1061, 0.1759
$\mathbf{b}_0$	1, 0, 5	0.31, 0.91, 3.50
$\mathbf{b}_1$	1, 15, 7.5	1.24, 14.80, 8.09
θ_2~θ_5 [deg]	2, 4, 6, 8	4.68, 20.83, 32.63, 38.60
α_2~α_5 [deg]	3, 6, 9, 12	−0.89, −3.07, −3.55, −3.36

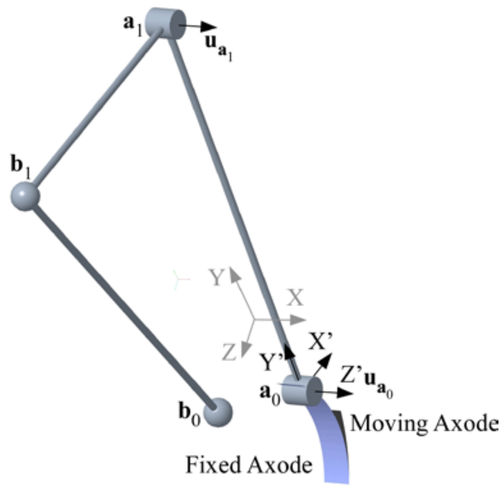

Fig. 8. Synthesized RRSS linkage with fixed and moving axode sections

Table 8. Tibial position coordinates achieved by the synthesized RRSS linkage

Pos.	$\mathbf{p}^*$ [mm]	$\mathbf{q}^*$ [mm]	$\mathbf{r}^*$ [mm]
1	−12.44, 38.45, 184.26	31.51, 35.63, 185.49	33.21, 39.85, 131.59
2	−11.56, 26.44, 186.64	32.42, 24.06, 187.40	33.67, 31.78, 133.87
3	−6.99, −18.59, 188.38	37.06, −19.07, 187.65	36.35, 1.09, 137.47
4	−1.90, −54.37, 181.61	42.11, −53.09, 180.03	39.54, −23.72, 134.68
5	1.32, −72.96, 174.95	45.27, −70.67, 173.06	41.60, −36.76, 131.07

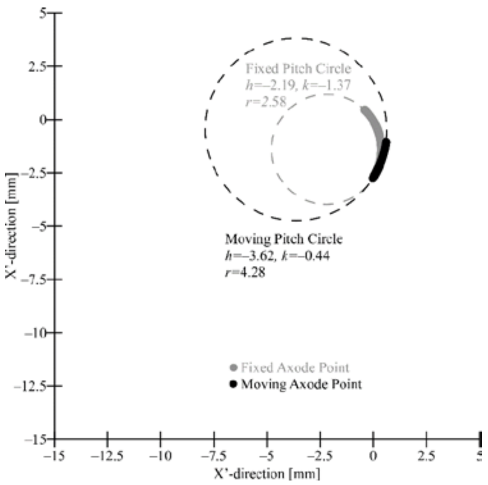

Fig. 9. RRSS linkage fixed and moving axode points (in X'-Y' plane) and gear pitch circles

Table 9. Tibial position coordinates achieved by the transfemoral prosthetic knee with circular gears

Pos.	$\mathbf{p}^*$ [mm]	$\mathbf{q}^*$ [mm]	$\mathbf{r}^*$ [mm]
1	−12.44, 38.45, 184.26	31.51, 35.63, 185.49	33.21, 39.85, 131.59
2	−11.55, 26.61, 186.45	32.44, 24.23, 187.21	33.69, 31.88, 133.68
3	−6.90, −18.50, 187.82	37.15, −18.98, 187.09	36.44, 1.18, 136.90
4	−1.75, −54.48, 180.88	42.25, −53.19, 179.30	39.66, −23.73, 134.00
5	1.30, −72.21, 174.58	45.26, −69.94, 172.70	41.62, −36.15, 130.61

Using Knee Motion Data from Zeng et. al. (severe KOA)

Table 10 includes both the initial and calculated dimensions from the authors' RRSS motion generation model. The precision positions used in this example appear in Table 11 in the part 1 work. Table 10 represents both the output from the second stage and the input for the third stage in the authors' knee design method. The synthesized RRSS linkage is illustrated in Figure 10 and the tibia position coordinates achieved by this linkage are included in Table 11.

In Figure 11, the fixed and moving axode points are illustrated in the X'-Y' plane. These points were calculated using Equation (2). In Fig. 10, the spatial representations of the fixed and moving axode sections are also illustrated. The X'-Y' plane axode point coordinates represent both the output from the third stage and the input for the fourth stage in the authors' knee design method.

Figure 11 also includes the calculated pitch circle dimensions. These circle dimensions represent the output from the fourth stage in the authors' knee design method and are used in gear selection for the prosthetic knee. The tibia position coordinates (also represented by $\mathbf{p}_j^*$, $\mathbf{q}_j^*$ and $\mathbf{r}_j^*$) achieved by circular gears with calculated pitch circle dimensions are included in Table 12.

Table 10. Initial and calculated RRSS linkage dimensions

Variable	Initial Value	Calculated Value
$\mathbf{a}_0$	1, 0, 0	1.26, −0.07, 1.251
$\mathbf{a}_1$	1, 10, 0	0.57, 9.78, 0.31
$\mathbf{u}_{\mathbf{a}_0}$	1, 0, 0	0.9464, 0.0955, 0.3086
$\mathbf{u}_{\mathbf{a}_1}$	1, 0, 0	0.9464, 0.0955, 0.3086
$\mathbf{b}_0$	1, 0, 5	1.37, 1.45, 3.49
$\mathbf{b}_1$	1, 15, 7.5	0.74, 14.36, 7.41
θ_2~θ_5 [deg]	2, 4, 6, 8	0.01, 12.32, 22.99, 28.65
α_2~α_5 [deg]	3, 6, 9, 12	−0.00, −3.38, −5.42, −6.06

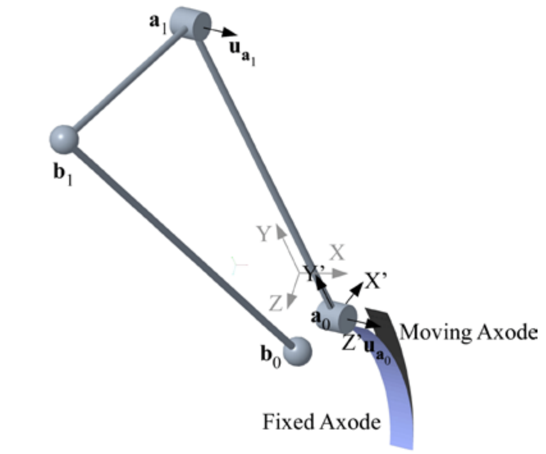

Fig. 10. Synthesized RRSS linkage with fixed and moving axode sections

Table 11. Tibial position coordinates achieved by the synthesized RRSS linkage

Pos.	$\mathbf{p}^*$ [mm]	$\mathbf{q}^*$ [mm]	$\mathbf{r}^*$ [mm]
1	−20.41, 27.23, 188.11	23.26, 21.93, 190.55	27.14, 30.05, 137.21
2	−20.41, 27.21, 188.11	23.26, 21.91, 190.55	27.14, 30.04, 137.21
3	−18.39, −1.64, 190.88	25.51, −5.09, 192.02	28.02, 10.95, 140.42
4	−15.05, −29.53, 189.25	28.98, −31.03, 189.40	29.85, −7.74, 140.58
5	−12.50, −45.45, 186.37	31.55, −45.75, 186.08	31.34, −18.50, 139.35

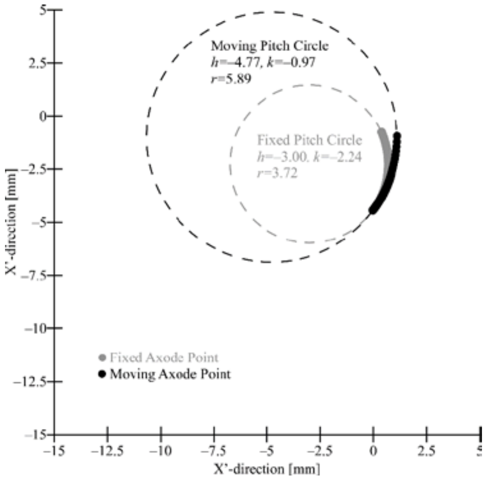

Fig. 11. RRSS linkage fixed and moving axode points (in X’-Y’ plane) and gear pitch circles

Table 12. Tibial position coordinates achieved by the transfemoral prosthetic knee with circular gears

Pos.	$\mathbf{p}^*$ [mm]	$\mathbf{q}^*$ [mm]	$\mathbf{r}^*$ [mm]
1	−20.41, 27.23, 188.11	23.26, 21.93, 190.55	27.14, 30.05, 137.21
2	−20.41, 27.23, 188.11	23.26, 21.93, 190.55	27.14, 30.05, 137.21
3	−18.33, −1.59, 190.65	25.58, −5.01, 191.77	28.06, 11.16, 140.21
4	−14.97, −29.40, 188.95	29.07, −30.83, 189.07	29.87, −7.28, 140.38
5	−12.46, −45.13, 186.12	31.60, −45.34, 185.81	31.30, −17.81, 139.25

Using Knee Motion Data from Zheng et. al. (medial KM)

Table 13 includes both the initial and calculated dimensions from the authors’ RRSS motion generation model. The precision positions used in this example appear in Table 12 in the part 1 work. Table 13 represents both the output from the second stage and the input for the third stage in the authors’ knee design method. The synthesized RRSS linkage is illustrated in Figure 12 and the tibia position coordinates achieved by this linkage are included in Table 14.

In Figure 13, the fixed and moving axode points are illustrated in the X’-Y’ plane. These points were calculated using Equation (2). In Fig. 12, the spatial representations of the fixed and moving axode sections are also illustrated. The X’-Y’ plane axode point coordinates represent both the output from the third stage and the input for the fourth stage in the authors’ knee design method.

Figure 13 also includes the calculated pitch circle dimensions. These circle dimensions represent the output from the fourth stage in the authors’ knee design method and are used in gear selection for the prosthetic knee. The tibia position coordinates (also represented by $\mathbf{p}_j^*$, $\mathbf{q}_j^*$ and $\mathbf{r}_j^*$) achieved by circular gears with calculated pitch circle dimensions are included in Table 15.

Table 13. Initial and calculated RRSS linkage dimensions

Variable	Initial Value	Calculated Value
$\mathbf{a}_0$	1, 0, 0	0.34, 1.00, 0.64
$\mathbf{a}_1$	1, 10, 0	1.55, 8.73, 0.63
$\mathbf{u}_{\mathbf{a}_0}$	1, 0, 0	0.9759, −0.1527, 0.1562
$\mathbf{u}_{\mathbf{a}_1}$	1, 0, 0	0.9759, −0.1527, 0.1562
$\mathbf{b}_0$	1, 0, 5	1.32, 0.90, 2.37
$\mathbf{b}_1$	1, 15, 7.5	1.07, 15.57, 7.87
θ_2~θ_5 [deg]	2, 4, 6, 8	7.77, 25.05, 55.26, 61.44
α_2~α_5 [deg]	3, 6, 9, 12	−2.53, −7.98, −15.37, −16.18

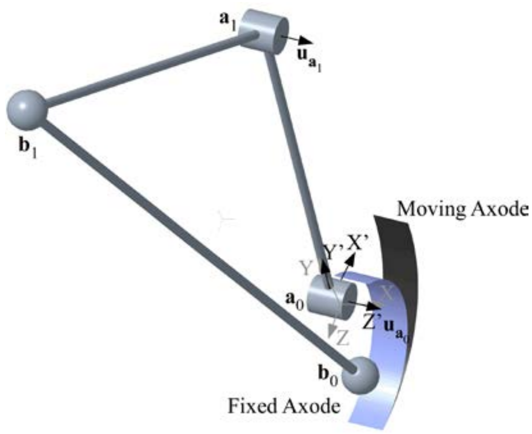

Fig. 12. Synthesized RRSS linkage with fixed and moving axode sections

Table 14. Tibial position coordinates achieved by the synthesized RRSS linkage

Pos.	$\mathbf{p}^*$ [mm]	$\mathbf{q}^*$ [mm]	$\mathbf{r}^*$ [mm]
1	−14.88, 65.56, 146.88	29.00, 62.64, 149.45	31.60, 55.86, 95.84
2	−17.85, 52.01, 152.15	26.04, 49.47, 155.08	29.45, 47.53, 101.13
3	−24.02, 19.77, 159.24	19.82, 17.96, 163.12	24.81, 26.98, 110.02
4	−33.01, −43.95, 153.08	10.62, −44.95, 159.11	17.45, −16.17, 113.82
5	−34.41, −58.25, 147.88	9.14, −59.19, 154.45	16.15, −26.30, 112.08

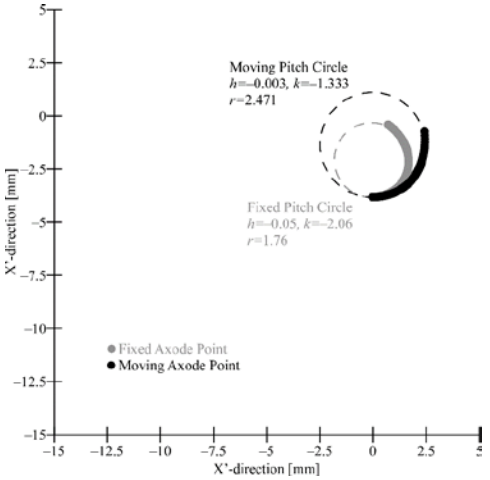

Fig. 13. RRSS linkage fixed and moving axode points (in X'-Y' plane) and gear pitch circles

Table 15. Tibial position coordinates achieved by the transfemoral prosthetic knee with circular gears

Pos.	$\mathbf{p}^*$ [mm]	$\mathbf{q}^*$ [mm]	$\mathbf{r}^*$ [mm]
1	−14.88, 65.56, 146.88	29.00, 62.64, 149.45	31.60, 55.86, 95.84
2	−17.79, 52.17, 151.95	26.10, 49.62, 154.88	29.50, 47.64, 100.93
3	−23.99, 19.60, 158.87	19.86, 17.80, 162.77	24.86, 26.98, 109.70
4	−32.89, −43.51, 152.79	10.74, −44.51, 158.84	17.58, −15.55, 113.67
5	−34.32, −57.85, 147.71	9.23, −58.79, 154.30	16.24, −25.69, 112.10

Using Knee Motion Data from Zheng et. al. (lateral KM)

Table 16 includes both the initial and calculated dimensions from the authors' RRSS motion generation model. The precision positions used in this example appear in Table 13 in the part 1 work. Table 16 represents both the output from the second stage and the input for the third stage in the authors' knee design method. The synthesized RRSS linkage is illustrated in Figure 14 and the tibia position coordinates achieved by this linkage are included in Table 17.

In Figure 15, the fixed and moving axode points are illustrated in the X'-Y' plane. These points were calculated using Equation (2). In Fig. 14, the spatial representations of the fixed and moving axode sections are also illustrated. The X'-Y' plane axode point coordinates represent both the output from the third stage and the input for the fourth stage in the authors' knee design method.

Figure 15 also includes the calculated pitch circle dimensions. These circle dimensions represent the output from the fourth stage in the authors' knee design method and are used in gear selection for the prosthetic knee. The tibia position coordinates (also represented by $\mathbf{p}_j^*$, $\mathbf{q}_j^*$ and $\mathbf{r}_j^*$) achieved by circular gears with calculated pitch circle dimensions are included in Table 18.

Table 16. Initial and calculated RRSS linkage dimensions

Variable	Initial Value	Calculated Value
$\mathbf{a}_0$	1, 0, 0	−0.30, 6.63, 3.89
$\mathbf{a}_1$	1, 10, 0	−0.88, 8.43, −0.22
$\mathbf{u}_{\mathbf{a}_0}$	1, 0, 0	0.9916, 0.0324, −0.1253
$\mathbf{u}_{\mathbf{a}_1}$	1, 0, 0	0.9916, 0.0324, −0.1253
$\mathbf{b}_0$	1, 0, 5	2.15, 1.23, 3.19
$\mathbf{b}_1$	1, 15, 7.5	2.95, 11.25, 5.21
θ_2~θ_5 [deg]	5, 10, 15, 20	17.70, 27.87, 43.88, 48.65
α_2~α_5 [deg]	−3, −6, −9, −12	−3.56, −6.44, −12.14, −14.11

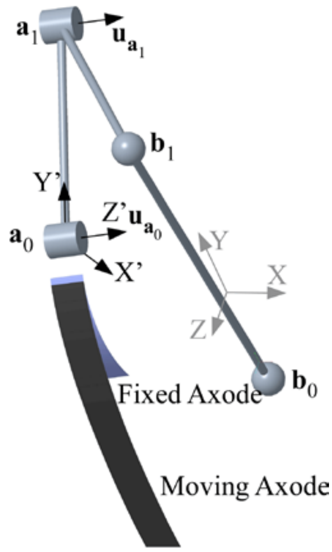

Fig. 14 Synthesized RRSS linkage with fixed and moving axode sections

Table 17. Tibial position coordinates achieved by the synthesized RRSS linkage

Pos.	$\mathbf{p}^*$ [mm]	$\mathbf{q}^*$ [mm]	$\mathbf{r}^*$ [mm]
1	1.00, 15.61, 169.22	44.93, 12.60, 167.82	44.14, 26.52, 115.56
2	1.98, −24.55, 166.63	45.79, −28.43, 164.03	45.22, −2.24, 116.71
3	2.00, −44.66, 161.57	45.73, −48.87, 158.29	45.44, −16.93, 114.63
4	1.47, −71.70, 150.34	45.08, −76.22, 146.02	45.35, −37.03, 108.74
5	1.21, −78.67, 146.52	44.79, −83.23, 141.91	45.24, −42.29, 106.57

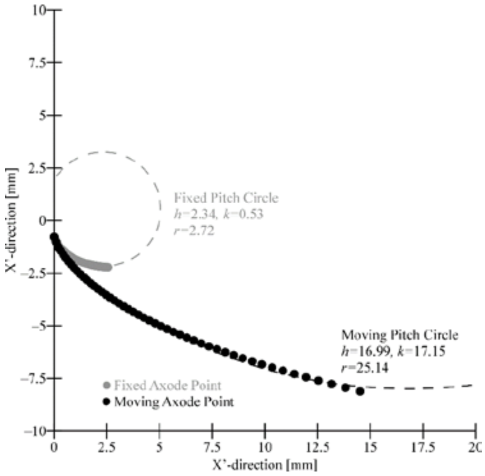

Fig. 15. RRSS linkage fixed and moving axode points (in X'-Y' plane) and gear pitch circles

Table 18. Tibial position coordinates achieved by the transfemoral prosthetic knee with circular gears

Pos.	$\mathbf{p}^*$ [mm]	$\mathbf{q}^*$ [mm]	$\mathbf{r}^*$ [mm]
1	1.00, 15.61, 169.22	44.93, 12.60, 167.82	44.14, 26.52, 115.56
2	1.97, −24.51, 166.50	45.78, −28.39, 163.91	45.20, −2.28, 116.54
3	1.97, −44.52, 161.35	45.70, −48.73, 158.08	45.40, −16.92, 114.33
4	1.40, −71.48, 149.88	45.01, −75.99, 145.58	45.27, −36.98, 108.11
5	1.15, −77.93, 146.24	44.73, −82.49, 141.68	45.16, −41.85, 105.99

Using Knee Motion Data from Li et. al.

Table 16 includes both the initial and calculated dimensions from the authors' RRSS motion generation model. The precision positions used in this example appear in Table 14 in the part 1 work. Table 16 represents both the output from the second stage and the input for the third stage in the authors' knee design method. The synthesized RRSS linkage is illustrated in Figure 16 and the tibia position coordinates achieved by this linkage are included in Table 17.

In Figure 17, the fixed and moving axode points are illustrated in the X'-Y' plane. These points were calculated using Equation (2). In Fig. 16, the spatial representations of the fixed and moving axode sections are also illustrated. The X'-Y' plane axode point coordinates represent both the output from the third stage and the input for the fourth stage in the authors' knee design method.

Figure 17 also includes the calculated pitch circle dimensions. These circle dimensions represent the output from the fourth stage in the authors' knee design method and are used in gear selection for the prosthetic knee. The tibia position coordinates (also represented by $\mathbf{p}_j^*$, $\mathbf{q}_j^*$ and $\mathbf{r}_j^*$) achieved by circular gears with calculated pitch circle dimensions are included in Table 18.

Table 19. Initial and calculated RRSS linkage dimensions

Variable	Initial Value	Calculated Value
$\mathbf{a}_0$	1, 0, 0	2.29, −1.13, 1.24
$\mathbf{a}_1$	1, 10, 0	1.55, 8.98, 1.57
$\mathbf{u}_{\mathbf{a}_0}$	1, 0, 0	0.9941, 0.0753, −0.0782
$\mathbf{u}_{\mathbf{a}_1}$	1, 0, 0	0.9941, 0.0753, −0.0782
$\mathbf{b}_0$	1, 0, 5	1.11, 2.89, 2.53
$\mathbf{b}_1$	1, 15, 7.5	−0.78, 12.93, 7.78
θ_2~θ_5 [deg]	5, 10, 15, 20	1.35, 1.41, 4.89, 9.74
α_2~α_5 [deg]	3, 6, 9, 12	0.32, 0.34, 1.46, 3.74

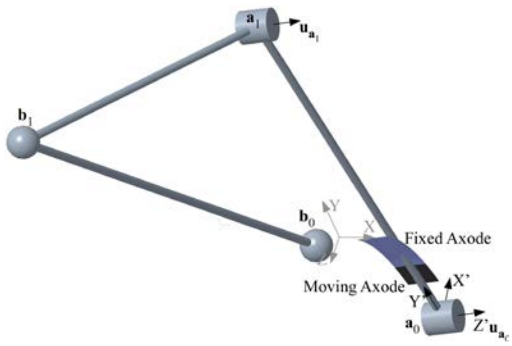

Fig. 16. Synthesized RRSS linkage with fixed and moving axode sections

Table 20. Tibial position coordinates achieved by the synthesized RRSS linkage

Pos.	$\mathbf{p}^*$ [mm]	$\mathbf{q}^*$ [mm]	$\mathbf{r}^*$ [mm]
1	−28.01, 23.99, 217.91	15.89, 22.92, 221.47	20.31, 30.75, 168.13
2	−27.49, 17.79, 218.55	16.41, 16.51, 221.98	20.74, 25.87, 168.88
3	−27.46, 17.48, 218.58	16.44, 16.19, 222.00	20.76, 25.63, 168.91
4	−26.10, 0.27, 219.36	17.81, −1.55, 222.39	21.89, 12.07, 170.20
5	−24.22, −26.29, 217.75	19.70, −28.88, 220.09	23.46, −8.96, 169.94

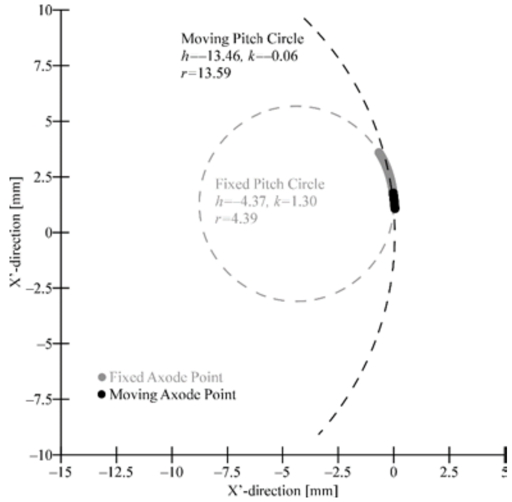

Fig. 17. RRSS linkage fixed and moving axode points (in X'-Y' plane) and gear pitch circles

Table 21. Tibial position coordinates achieved by the transfemoral prosthetic knee with circular gears

Pos.	$\mathbf{p}^*$ [mm]	$\mathbf{q}^*$ [mm]	$\mathbf{r}^*$ [mm]
1	−28.01, 23.99, 217.91	15.89, 22.92, 221.47	20.31, 30.75, 168.13
2	−27.62, 19.41, 218.43	16.28, 18.18, 221.89	20.63, 27.17, 168.73
3	−27.33, 15.86, 218.76	16.58, 14.52, 222.15	20.87, 24.39, 169.14
4	−26.09, 0.30, 219.52	17.83, −1.54, 222.54	21.90, 12.18, 170.38
5	−24.17, −26.55, 218.11	19.75, −29.16, 220.42	23.50, −8.98, 170.38

Summary of Knee Motion Accuracy

Figure 18 includes error plots between circular gears and noncircular gears at each tibia position. The tibia positions achieved by the noncircular gears are identical to those achieved by their corresponding RRSS linkages. The error values were calculated using Equation (1) for each example problem. Except for Examples 5.2 and 5.5, tibial motion using circular gears outperformed noncircular gears in terms of the error sum. In Example 5.2, noncircular gears are more accurate by only 0.34%. This example is reflected in the tibia position error plot for *Zhang et. al.* in Fig. 18. In Example 5.5, noncircular gears are more accurate by 7.95% -but this is largely due to the error at position 5. This example is reflected in the tibia position error plot for *Zheng et. al. (medial KM)* in Fig. 18. While circular gears are preferred over noncircular gears in terms of cost and design simplicity, Fig. 18 shows that circular gears also offer little to no loss in tibial position accuracy compared to noncircular gears.

So, while tibial position accuracy using circular gears was shown to be at least comparable to noncircular gears using the empirical data from Benoit et. al. (Lee et al. 2020), the same conclusion can be reached from this study. And unlike the knee motion data from Benoit et. al, the data used in this study reflect knee motion distinctions due to gender, age, nationality, body mass, gait speed and knee condition.

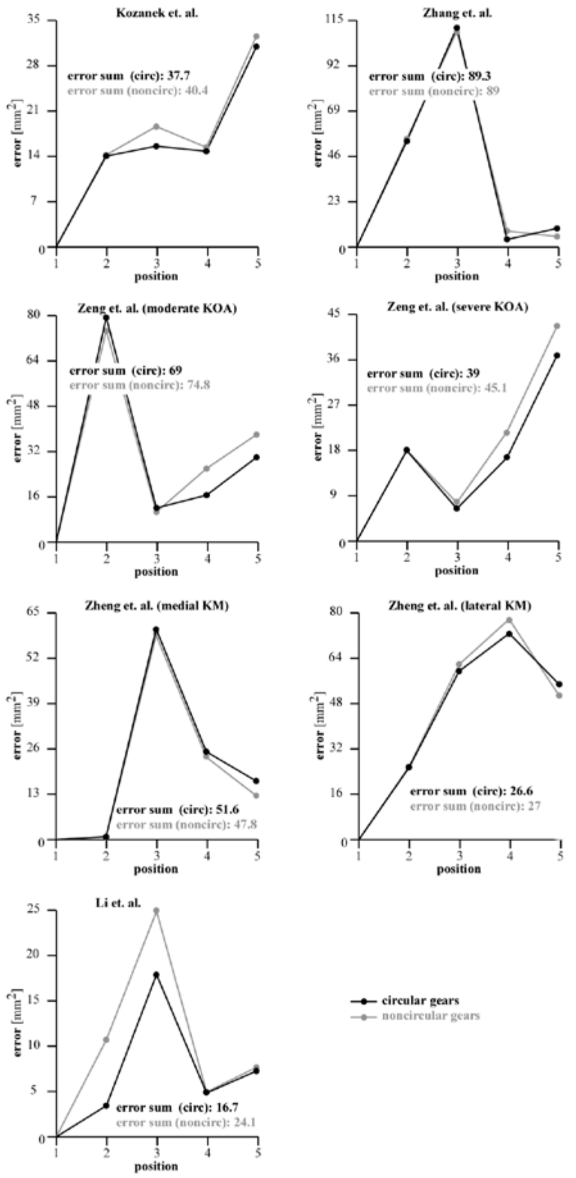

Fig. 18. Tibia position error plots using circular and noncircular gears for each knee motion data set

DISCUSSION

In the authors' design method for a gear-based transfemoral prosthetic knee, the moving axode produced the external gear and the fixed axode produced the internal gear (Lee et al. 2020). The rolling motion of an external gear within an internal gear is *polycentric* or *complex* motion. In each of the examples in this work however, the moving axodes produce internal gears and the fixed axodes produce external gears. The rolling motion of an internal gear over an external gear is *pure rotation*.

Given pure rotation, a revolute joint can be used instead if the joint axis is aligned with the center axis of the external gear. The primary reason why the examples in this work consistently produced internal moving axode gears and fixed axode external gears is due to the initial values specified for $\mathbf{a}_0$, $\mathbf{a}_1$, $\mathbf{b}_0$ and $\mathbf{b}_1$ for RRSS motion generation. These values are virtually unchanged in each example but they are dissimilar from the values used to produce the gears in the work of Lee et al (2020). With different initial values specified for $\mathbf{a}_0$, $\mathbf{a}_1$, $\mathbf{b}_0$ and $\mathbf{b}_1$, different RRSS configurations are calculated in motion generation and subsequently different axode curves are calculated in axode generation.

CONCLUSION

This work is the second part of a two-part work where the authors' design method for gear-based transfemoral prosthetic knees is used to determine if circular gears are comparable to noncircular gears (in terms of tibial position accuracy) in a transfemoral prosthetic knee. The 7 groups tibial positions produced in the part 1 work were used in the authors' design method. It was observed that the tibial position accuracy using circular gears was at least comparable to noncircular gears. Subsequently, the authors' design method is not a specialized method, but it was equally effective using data from clinical studies that consider factors such as participant age, gender, nationality, body mass, gait speed and knee condition.

REFERENCES

Kozánek, M., Hosseini, A., Liu, F., Van, de Velde S. K., Gill, T. J., Rubash, H. E. and Li, G., "Tibiofemoral Kinematics and Condylar Motion during the Stance Phase of Gait,"; Journal of Biomechanics, Vol.42, No.12, pp. 1877-1884(2009).

Lee, W., "An Evaluation of Spatial and Spherical Motion Generation for Application in Knee Motion Analysis and Simulation,"; Journal of the Chinese Society of Mechanical Engineers, Vol. 41, No. 2, pp. 221-228(2020).

Lee, W., Russell, K. and Sodhi, R. S., "On Transfemoral Prosthetic Knee Design for Natural Human Knee Motion,"; Recent Patents on Mechanical Engineering, Vol.13, No.1, pp. 49-59(2020).

Lee, W., Russell, K., D'Alessio, J. and Sodhi, R. S., "Method of Designing and Manufacturing Artificial Joint,"; TW Patent I642419(2018).

Li, J., Tsai, T., Felson, D. T., Li, G. and Lewis, C. L., "Six Degree-of-Freedom Knee Joint Kinematics in Obese Individuals with Knee Pain during Gait,"; PLoS ONE. Vol.12, No.3, pp. e0174663(2017).

Li, J., Tsai, T., Felson, D. T., Li, G. and Lewis, C. L., "Correction: Six Degree-of-Freedom Knee Joint Kinematics in Obese Individuals with Knee Pain during Gait,"; PLoS ONE. Vol.14, No.2, pp. e0213084(2019).

Russell K. and Shen Q., "Expanded Spatial Four-Link Motion and Path Generation with Order and Branch Defect Elimination,"; Inverse Problems in Science and Engineering, Vol. 21, No. 1, pp. 129-140 (2013).

Shen Q., Russell K., Lee W. and Sodhi R. S., "On Cam System Design to Replicate Spatial Four-Bar Mechanism Coupler Motion,"; Inverse Problems in Science and Engineering, Vol. 19, No. 2, pp. 251-265 (2011).

Zeng, X., Ma, L., Lin, Z., Huang, W., Huang, Z., Zhang, Y. and Mao, C., "Relationship Between Kellgren-Lawrence Score and 3D Kinematic Gait Analysis of Patients with Medial Knee Osteoarthritis Using a New Gait System,"; Scientific Reports. Vol.7, No.1, pp. 4080(2017).

Zhang, Y., Yao, Z., Wang, S., Huang, W., Ma, L, Huang, H., and Xia, H., "Motion Analysis of Chinese Normal Knees during Gait Based on a Novel Portable System,"; Gait Posture, Vol.41, No.3, pp. 763-768(2015).

Zheng, L., Carey, R., Thorhauer, E., Tashman, S., Harner, C. and Zhang, X., "In Vivo Tibiofemoral Skeletal Kinematics and Cartilage Contact Arthrokinematics During Decline Walking After Isolated Meniscectomy,"; Medical Engineering and Physics, Vol.51, pp. 41-48(2018).

經股人工膝關節使用圓形與非圓形齒輪進行脛骨運動精度的研究　第二部分：運動軌跡與瞬軸面的生成和曲線擬合

李文宗

國立屏東科技大學 生物機電工程學系

羅素凱文　索德　里拉兹

紐澤西理工學院 機械與工業工程學系

摘要

這是兩個相關研究的第二部分。作者們使用七項臨床膝關節運動研究的膝關節運動數據，示範應

用齒輪為基礎的經股人工膝關節的設計方法。這兩個相關研究的主要目是測試圓形齒輪與非圓形齒輪在經股人工膝關節的步態過程中，是否都能夠始終如一地表現出準確的脛骨運動。在第二部分中，計算雙旋轉-雙球面對(RRSS)空間機構以趨近於第一部分中所產生的脛骨運動位置。生成這些連桿的瞬軸面，計算圓尺寸以最佳適合於瞬心軌跡。這些圓成為人工膝關節設計中雙齒輪對的齒節圓。最後，對使用圓形齒輪與非圓形齒輪的人工膝蓋設計方法進行脛骨運動位置精度的比較。與需要客制化的非圓形齒輪不同的地方，圓形齒輪在製造成本和設計簡易性方面均具有優勢，因為它是屬於標準製造的零件。然而，為了證明在膝關節設計中使用圓形齒輪是合適的，必須確定它是否可以始終如一地表現出與非圓形齒輪一樣準確的脛骨運動。